0026-895X/04/6504-860–867$20.00
MOLECULAR PHARMACOLOGY
Vol. 65, No. 4
2696/1137354
Mol Pharmacol 65:860–867, 2004
Printed in U.S.A.

Crystal Structures of the Mitochondrial Deoxyribonucleotidase in Complex with Two Specific Inhibitors

Agnes Rinaldo-Matthis, Chiara Rampazzo, Jan Balzarini, Peter Reichard, Vera Bianchi, and Pär Nordlund

Department of Biochemistry and Biophysics, Stockholm University, Stockholm, Sweden (A.R.-M., P.N.); Department of Biology, University of Padova, Padova, Italy (C.R., P.R., V.B.); Rega Institute for Medical Research, Katholieke Universiteit Leuven, Leuven, Belgium (J.B.); and Department of Biochemistry, Medical Nobel Institute, MBB, Stockholm, Sweden (P.R.)

Received June 2, 2003; accepted October 27, 2003

This article is available online at http://molpharm.aspetjournals.org

ABSTRACT

Monophosphate nucleotidases are enzymes that dephosphorylate nucleotides to their corresponding nucleosides. They play potentially important roles in controlling the activation of nucleotide-based drugs targeted against viral infections or cancer cells. The human mitochondrial deoxyribonucleotidase (dNT-2) dephosphorylates thymidine and deoxyuridine monophosphates. We describe the high resolution structures of the dNT-2 enzyme in complex with two potent nucleoside phosphonate inhibitors, (*S*)-1-[2′-deoxy-3′,5′-*O*-(1-phosphono) benzylidene-β-D-*threo*-pentofuranosyl]thymine (DPB-T) at 1.6-Å resolution and (±)-1-*trans*-(2-phosphonomethoxycyclopentyl)-uracil (PMcP-U) at 1.4-Å resolution. The mixed competitive inhibitor DPB-T and the competitive inhibitor PMcP-U both bind in the active site of dNT-2 but in distinctly different binding modes, explaining their different kinetics of inhibition. The pyrimidine part of the inhibitors binds with very similar hydrogen bond interactions to the protein but with their phosphonate moieties in different binding sites compared with each other and to the previously determined position of phosphate bound to dNT-2. Together, these phosphate/phosphonate binding sites describe what might constitute a functionally relevant phosphate entrance tunnel to the active site. The structures of the inhibitors in complex with dNT-2, being the first such complexes of any nucleotidase, might provide important information for the design of more specific inhibitors to control the activation of nucleotide-based drugs.

Seven different human 5′-nucleotidases have been cloned. One is an ecto enzyme anchored to the outer surface of the plasma membrane, five are soluble cytosolic proteins, and the last is a nuclear-encoded mitochondrial enzyme. All act on nucleoside monophosphates producing free nucleosides and inorganic phosphates. Both the base and the sugar determine the substrate efficiency of a nucleotide, but each natural nucleotide can be the substrate for more than one nucleotidase because the different enzymes have overlapping specificities. Conventional sequence comparisons do not directly account for the similar enzymatic properties of these enzymes. Among the seven nucleotidases, high sequence homology is found between the two AMP-preferring enzymes, CN-Ia and CN-Ib (Hunsucker et al., 2001; Sala-Newby and Newby, 2001) and the two deoxyribonucleotidases, cytosolic dNT-1 and mitochondrial dNT-2 (Rampazzo et al., 2000), whose genes have clearly arisen by a duplication event. The other three nucleotidases differ among themselves and relative to the previous four. Structural information is very important to clarify the functional homologies of this class of enzymes and to design synthetic substrates and inhibitors to modulate the in vivo function of nucleotidases. Recently, we determined the high-resolution structure of dNT-2 (Rinaldo-Matthis et al., 2002). The structure is composed of two domains, one α/β Rossman fold, and a truncated four-helix bundle. The active site is located in the interface between the two domains where a magnesium ion and a phosphate ion are bound in one structure. A structure with the product thymidine and BeF_3^- as a phosphate analog has also been determined. A major result from the structural study was that all intracellular human nucleotidases seem to have similar structural folds despite differences in sequence length. The structure of dNT-2 is most similar to that of phosphoserine phosphatase and belongs, together with the other intracellular human nucleotidases, to the protein structure group called the haloacid dehalogenase family (Rinaldo-Matthis et al., 2002). The ecto enzyme is instead different, being structurally related to, for example, *Escherichia coli* periplasmic

This work was supported by grants from Theleton Italia, Associazione Italiana per la Ricerca sul Cancro (to V.B.), the Swedish Research Council (to P.N.), the Swedish Cancer Society (to P.N.) and by European Commission grant QLGI-CT-2001-01004.

ABBREVIATIONS: dNT-2, deoxyribonucleotidase-2; DPB-T, (*S*)-1-[2′-deoxy-3′,5′-*O*-(1-phosphono)benzylidene-β-D-*threo*-pentofuranosyl]thymine; PMcP-U, (±)-1-*trans*-(2-phosphonomethoxycyclopentyl)uracil.

5′-nucleotidase (Knofel and Strater, 1999). The physiological function of nucleotidases is incompletely understood. The two deoxyribonucleotidases, dNT-1 and dNT-2, are especially active on thymidine and deoxyuridine monophosphates and are involved in the regulation of precursors for nuclear and mitochondrial DNA synthesis, respectively. They reverse the phosphorylation of thymidine and deoxyuridine made by cytosolic thymidine kinase TK1 and mitochondrial TK2, producing regulatory substrate cycles (Gazziola et al., 2001). Such cycles contribute to the modulation of deoxyribonucleotide pools and dampen potentially mutagenic pool imbalances. A clear example of the negative consequences of dTTP disregulation is the mitochondrial disease arising from genetic deficiency of thymidine phosphorylase, an enzyme of thymidine catabolism (Nishino et al., 1999). Besides their role in the regulation of physiological dNTP pools, substrate cycles between deoxyribonucleotidases and thymidine kinases may affect the therapeutic action of pyrimidine nucleoside analogs used as antiviral and antiblastic agents. The first step in the activation of these prodrugs is the phosphorylation catalyzed by deoxyribonucleoside kinases. If the monophosphates thus produced are reasonably good substrates for dNT-1 or another nucleotidase, the pharmacological efficiency of the analogs is reduced. Indeed, data from cultured cells indicate that high nucleotidase activity lowers the effect of the delivered analog (Carson et al., 1991; Schirmer et al., 1998; Dumontet et al., 1999). The higher instability of 3′-azido-2′,3′-dideoxythymidine monophosphate relative to dideoxy-4-thymidine (zidovudine) monophasphate in cells treated with membrane-permeable prodrugs (Balzarini et al., 2000) may also depend on their different efficiency as substrates for dNT-1 (Mazzon et al., 2003).

One possibility to overcome these potential problems could be to inhibit dNT-1. On the contrary, susceptibility of a nucleotide analog to the inactivating activity of dNT-2 could be important to avoid the mitochondrial toxicity of long-term treatments with nucleoside analogs, as is observed in HIV treatment with zidovudine. Zidovudine triphosphate is used by the mitochondrial DNA polymerase, with subsequent incorporation of the analog leading to severe mitochondrial toxicity (Lim and Copeland, 2001). Therefore, a deeper understanding of the structural basis for the substrate specificity of the nucleotidases, particularly dNT-2 and dNT-1, could be helpful for the design of improved variants of nucleoside analogs, which are good substrates for dNT-2 but not for dNT-1, thereby minimizing mitochondrial toxicity.

We here present crystal structures of dNT-2 in complex with the inhibitors DPB-T and PMcP-U. The inhibitors are synthetic phosphonate analogs that previously have been studied to differentiate between different nucleotidases in crude cell extracts, based on activity measurement. The nucleoside phosphonate analogs PMcP-U and DPB-T were shown to be strong inhibitors of dNT-2 with respect to the dephosphorylation of the substrate dUMP, whereas dNT-1 was inhibited only by PMcP-U (Mazzon et al., 2003).

Materials and Methods

Compounds DPB-T and PMcP-U were synthesized as described previously (Libosak et al., 1996; Endóva et al., 1998). Expression and purification of dNT-2 protein was performed as described previously (Rampazzo et al., 2000). Purified protein was maintained in 20 mM Tris-HCl, pH 7.5, 20% (v/v) glycerol, 2 mM dithiothreitol, 1 mM EDTA, and 13 mg/ml protein.

Crystallization. Crystals were obtained using the hanging drop vapor diffusion technique with a reservoir solution of 15 to 25% (w/v) polyethylene glycol 8000 and 50 mM KH_2PO_4, pH 5.3, in a drop made by mixing 1 μl of protein solution and 1 μl of reservoir solution. Crystals appeared after 3 days at room temperature and reached a maximum size of $0.3 \times 0.3 \times 0.3$ mm. The inhibitor complexes were achieved by soaking the crystals in a reservoir solution with 10 mM DPB-T and a 10 mM concentration of a racemic mixture of PMcP-U, each for 2 h.

Structure Determination and Refinement. Crystals belong to the space-group of $P4_32_12$ with cell dimensions a = 74 Å, b = 74 Å, and c = 106 Å, for both dNT-2-inhibitor complexes, containing one polypeptide per asymmetric unit. Data were collected on flash-frozen crystals after soaking the crystals in reservoir solution including 20% (v/v) glycerol. The data sets of the complexes of dNT-2 and the PMcP-U and the DPB-T inhibitors were collected at the European Synchrotron Radiation Facility (ESRF) at beam lines ID14.2 and ID14.4, respectively, diffracting to 1.4 and 1.6 Å.

Both data sets were processed using DENZO and SCALEPACK (Otwinowski and Wladek, 1997). The native dNT-2 structure previously determined was used for initial rigid-body refinement of the PMcP-U and DPB-T-data. The Fo-Fc maps produced showed clear electron density representing the PMcP-U and the DPB-T inhibitors. Crystallography & NMR System software (Brunger et al., 1998) was used for refinement of coordinates and B-factors of the DPB-T-structure complex, and REFMAC5 (Murshudov et al., 1997) was used for the refinement of the coordinates and B-factors of the PMcP-U structure complex. Anisotropic B-factor refinement was applied for the PMcP-U structure. The mean anisotropy (ratio of smallest and largest eigenvalues of the anisotropic displacement parameter matrix) is 0.744 for the protein, 0.676 for the solvent, and 0.716 for the ligands, with standard deviation of 0.1, 0.13, and 0.1, respectively. Despite the slightly higher value of mean anisotropy than expected in proteins with more than 50 residues (a mean value of 0.45) (Merritt, 1999), it caused a drop of around 4% in R and R_{free} values.

QUANTA (Accelrys, San Diego, CA) was used for model building. Solvent molecules were added using X-SOLVATE (Accelrys). Structural statistics are shown in Table 1.

The refinement of the PMcP-U structure converged at R_{cryst} and R_{free} of 13.3% and 16.5%, respectively. The final refinement of the DBP-dNT-2-T structure resulted in R_{cryst} and R_{free} of 18.6% and 20.6%. The models of the inhibitors were made using QUANTA and the parameter and topology files for the DPB-T inhibitor was made using HICUP (Kleywegt and Jones, 1998). REFMAC5 (Murshudov et al., 1997) was used to generate a library for the PMcP-U inhibitor. The quality of the final structures was verified using PROCHECK (Laskowski et al., 1993) The Ramachandran plot for the two inhibitors showed that for the DPB-T–dNT-2 structure, 91% of residues were in the most favorable regions and 9% were in the allowed regions. The PMcP-U structure complex had 94 and 6% in the most favorable regions and the allowed regions, respectively.

Coordinates and structure factors for dNT-2 complexed with PMcP-U and in complex with DPB-T have been deposited in the Protein Data Bank (accession codes 1Q92 and 1Q91, respectively).

Results

Structure Analysis. The binding modes of dNT-2 with PMcP-U and DPB-T were characterized by solving the 3D-structures by X-ray crystallography to 1.4 and 1.6 Å resolution, respectively. The overall structures of the dNT-2 inhibitor complexes are very similar to the phosphate-containing structure with a few small rearrangements of residues in the active site.

Binding Mode of PMcP-U to the Active Site of dNT-2. The refined model at 1.4 Å of the PMcP-U inhibitor complexed to dNT-2 comprises 193 residues, 341 water molecules, one Mg^{2+}, a glycerol molecule, and the PMcP-U molecule in the active site. The inhibitor was added as a racemic mixture (Fig. 1a), but the electron density revealed that only the (+) form was bound in the structure (Fig. 1b). The density for PMcP-U is very well defined in the first calculated map; after modeling the inhibitor into the electron density with subsequent refinement, the atomic B-factors for PMcP-U were low, the same as in the protein (~20 $Å^2$) suggesting nearly 100% occupancy. The model was refined to an R_{cryst} of 13.3% and an R_{free} of 16.5% (see Table 1 for details).

The binding of the phosphonate inhibitor PMcP-U resembles the binding of thymidine in the previously determined product complex (Rinaldo-Matthis et al., 2002). The uracil base of PMcP-U binds with hydrogen bond interactions similar to those of the thymine base in the product complex. Three water-mediated hydrogen bonds stabilize the position of uracil in the active site (Fig. 1c). The NH of uracil forms hydrogen bonds to Glu-50 via an H_2O and one of the carbonyls forms hydrogen bonds to Mg^{2+} via an H_2O. The other carbonyl oxygen of the uracil ring forms a hydrogen bond to the main chain amide nitrogen of Val-77 and to a water molecule, which is also hydrogen bonding to the main chain amide nitrogen and the OH of Ser-78 (Fig. 1d).

The phosphonate moiety of the inhibitor binds near Mg^{2+} and Asp-41, as does the phosphate in the phosphate-containing structure, although the phosphonate is translated 4 Å toward the surface of the protein compared with the phosphate in the phosphate-containing dNT-2 structure (Fig. 1c). Presumably, the different stereochemistry of the cyclopentyl that links the phosphonate to the base accounts for the different position occupied by the phosphonate compared with the phosphate in the phosphate-containing structure. The oxygens of the phosphonate are bound by several hydrogen bonds to the protein and to water molecules coordinated by the Mg^{2+} ion. One oxygen of the phosphonate of PMcP-U forms hydrogen bonds with a distance of 2.9 Å to the hydroxyl group of Ser-131, where the proton probably resides on the hydroxyl. The ammonium group of Lys-165 is probably the hydrogen bond acceptor in the interaction between the second oxygen of the phosphonate and Lys-165, with a distance of 2.9 Å. Two Mg^{2+}-coordinated water molecules stabilize oxygens of the phosphonate by hydrogen bonds of 2.7 Å each. There is no conformational change in the active site compared with the phosphate containing structure apart from the guanidinium group of Arg-163 at the entrance of the active site that has moved 4 Å (Fig. 1c).

TABLE 1
Crystallographic data collection and refinement statistics

	DPB-T	PMcP-U
Spacegroup	$P4_32_12$	$P4_32_12$
Unit cell dimensions (Å)		
$a = b$	73.6	73.8
c	106.8	106.0
Data collection statistics		
Resolution	20–1.7	30–1.4
I/σ (I)[a]	32 (7.7)	22 (2.4)
No. of observations	353,379	209,410
No of unique reflections	39,332	57,136
R_{merge} [a,b]	7.6(31)	5.8(31)
Completeness (%)[a]	100 (100)	98 (92)
Final refinement parameters		
Working R value[c]	18.6	13.3
No of reflections working set	34,625	40,132
Free R value[c]	20.6	16.5
Number of reflections test set	3859	4518
Number of non-H atoms in		
Protein molecule	1598	1598
Water	327	341
PMcP-U	19	
DPB-T	28	
Glycerol	6	
PO_4^{3-}	1	
Mg^{2+}	1	1
Root-mean-square deviation from ideal geometry of final models		
Bond lengths (Å)	0.02	0.02
Bond angles	2.2°	1.8°
Average B values ($Å^2$)	B value	Iso B_{eq} [d]
Protein	26	21
Ramachandran		
Most favored	92.9	94.2
Allowed	7.1	5.8

[a] Numbers in parantheses are for the highest resolution shell.
[b] $R_{sym} = (\Sigma_{hkl}\Sigma_i|I_i(hkl) - \langle I(hkl)\rangle|) / \Sigma_{hkl}\Sigma_i I_i(hkl))$ for n independent reflections and observations of a given reflection, $\langle I(hkl)\rangle$ is the average intensity of the i observation.
[c] $R_{cryst} = \Sigma_{hkl} |F_0(hkl) - F_c(hkl)| / \Sigma_h |F_0(hkl)|$
[d] $B_{eq} = 8\pi \times U_{eq}$

DPB-T Binding in the Active Site. The model of the DPB-T-dNT-2 complex comprises 193 residues and 334 water molecules, a magnesium, a molecule of DPB-T inhibitor, and a phosphate ion bound in the active site (Fig. 2). Density for DPB-T was unambiguous, and the molecule could be modeled with full occupancy with B-factors similar to the protein (~20 $Å^2$). The model was refined to an R_{cryst} of 18.6% and an R_{free} of 20.6%. Relevant data for data collection and refinement statistics are summarized in Table 1.

In the DPB-T-dNT-2 structure complex, Trp-76 has moved 1.7 Å away from the inhibitor compared with the PMcP-U product complex, presumably to accommodate the larger ring systems of DPB-T (data not shown). The thymine base of DPB-T binds in the same place as the uracil base of PMcP-U but it is inverted 180° though keeping the same hydrogen-bond interactions of the base carbonyl oxygen with residues in the active site (Fig. 1c and 2c). A carbonyl of the thymine forms hydrogen bonds to an Mg^{2+}-coordinated water with a distance of 2.8 Å. The amide of the base forms hydrogen bonds both to the carbonyl oxygen of Phe-75 (3.3 Å) and to Glu-50 via water at a distance of 2.6 Å. The second carbonyl of the thymine base forms hydrogen bonds to the amide of Val-77 at a distance of 2.6 Å and to Ser-78 via a water molecule. The rest of the DPB-T molecule is oriented toward the solvent. One oxygen of the phospho moiety of DPB-T is interacting with a hydrogen bond (2.8 Å) to the NE1 of Trp-96 via a water molecule (Fig. 2d). Trp-96 is also stabilizing the pentofuranosyl part of the inhibitor by aromatic stacking interactions. The phosphonate moiety of DPB-T makes hydrogen bond interactions with the positively charged residues Lys-134 and Arg-163 on the surface of the protein (i.e., the phosphonate binding site differs from that of PMcP-U (Fig. 2, c and d). The guanidinium group of Arg-163 has moved 3.5 Å compared with the PMcP-U structure and stabilizes two oxygens of the phosphonate with hydrogen bonds (Fig. 2c). Lys-134 forms a hydrogen bond to one oxygen of the phosphonate moiety; another oxygen is hydrogen bonding to water at the surface of the protein. In addition to the DPB-T inhibitor, the active site contains a phosphate group in the same position as the phosphate in the phosphate containing dNT-2 structure. It is coordinated by the Mg^{2+} ion and forms

an extensive hydrogen bonding network to the amide nitrogens of residues Met-42 (data not shown), Asp-43 and Ser-131 and the side chains of Lys-165 (data not shown), Asp-43, and three water molecules.

Discussion

The complexes of the inhibitors with dNT-2 now provide a structural basis for explaining their kinetics. The kinetics of

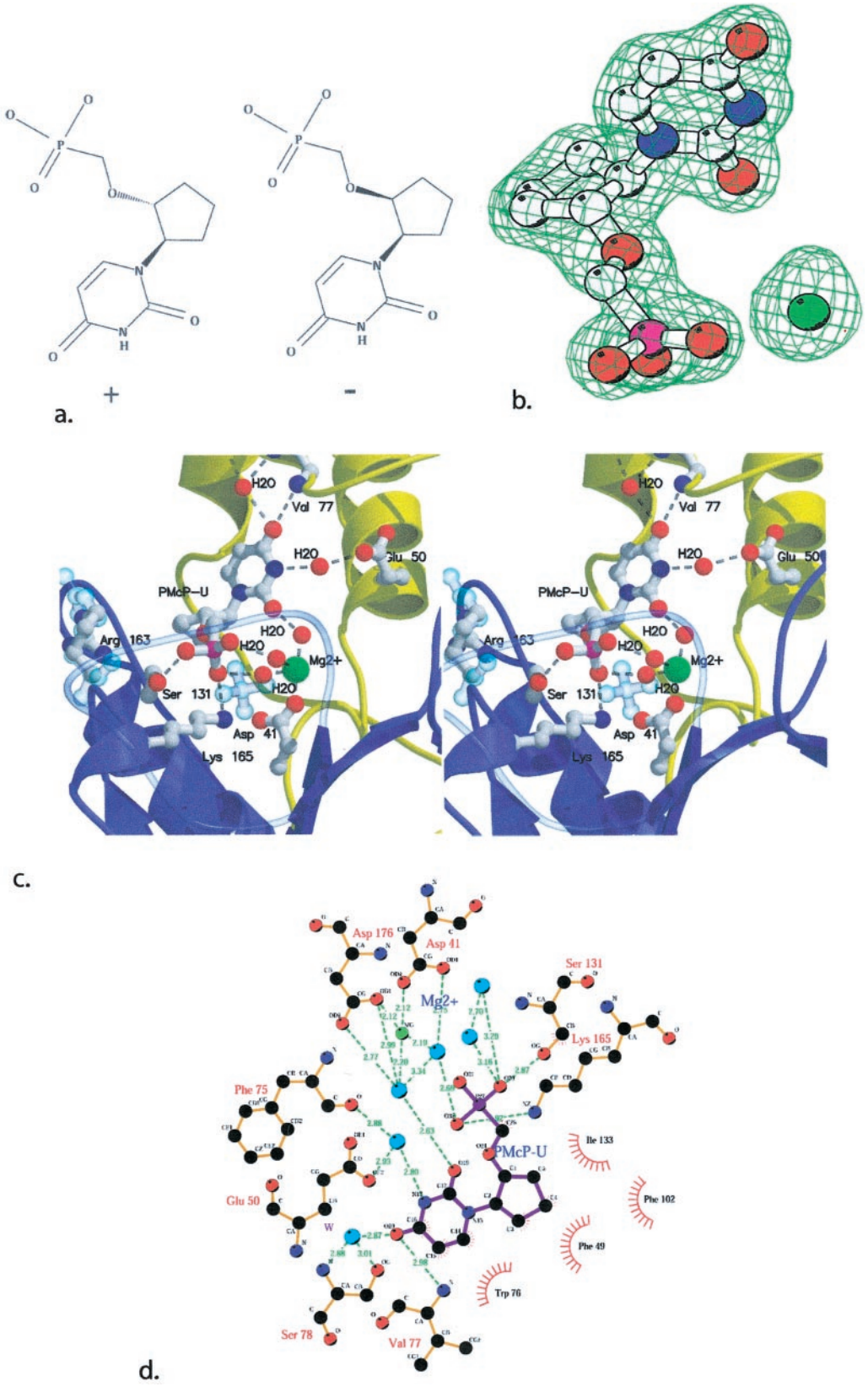

Fig. 1. a, structural formulas of PMcP-U. b, omit map contoured at 3σ of the PMcP-U inhibitor and the Mg^{2+} in the active site of dNT-2 (colored by atom type: red, oxygen; blue, nitrogen; white, carbon). c, detailed stereo view of the active site of dNT-2 with bound PMcP-U inhibitor. In light blue, the phosphate and Arg163 seen in the phosphate containing dNT-2 structure (Rinaldo-Matthis et al., 2002). d, schematic picture of dNT-2 complexed with Mg^{2+} and PMcP-U showing specificity determinants for product binding.

the inhibition of dNT-2 by the two compounds studied in the present work is different (Rampazzo et al., 2002). The differences can now be addressed through the high-resolution structures. The kinetic analysis revealed PMcP-U to be a competitive inhibitor of dNT-2 (Mazzon et al., 2003). This is fully consistent with the structure of the dNT-2-PMcP-U complex, where PMcP-U binds in a manner quite similar to that expected from the substrate based on our thymidine-dNT-2 structure, and where the three moieties (the base, the cyclopentyl, and the phosphono moiety) all overlap when the

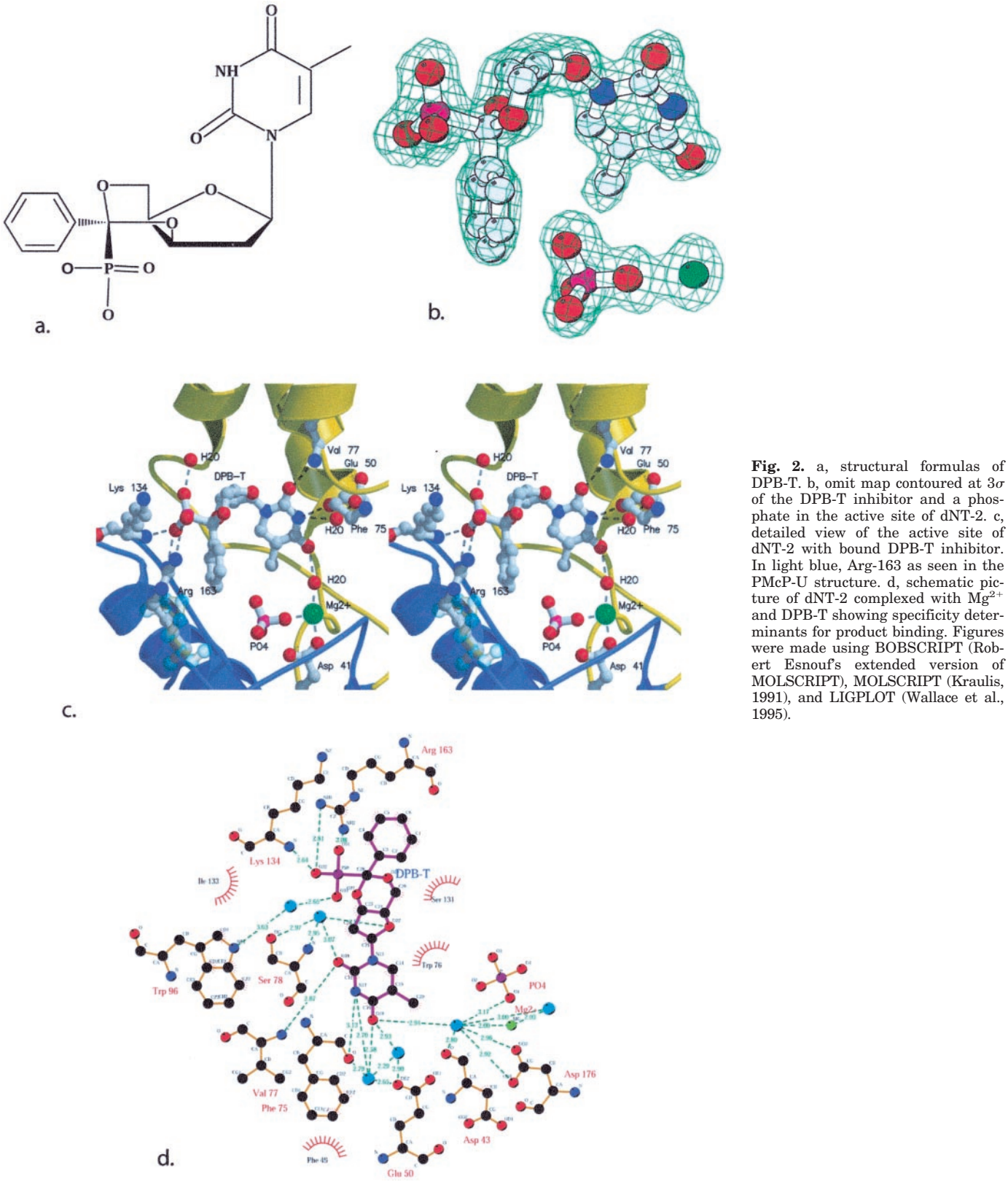

Fig. 2. a, structural formulas of DPB-T. b, omit map contoured at 3σ of the DPB-T inhibitor and a phosphate in the active site of dNT-2. c, detailed view of the active site of dNT-2 with bound DPB-T inhibitor. In light blue, Arg-163 as seen in the PMcP-U structure. d, schematic picture of dNT-2 complexed with Mg^{2+} and DPB-T showing specificity determinants for product binding. Figures were made using BOBSCRIPT (Robert Esnouf's extended version of MOLSCRIPT), MOLSCRIPT (Kraulis, 1991), and LIGPLOT (Wallace et al., 1995).

PMcP-U structure is compared with the thymidine bound structure. The inhibitory effect of PMcP-U depends on the inertness of the nonhydrolyzable phosphonate bond. In addition, according to what has been seen earlier in the structures with phosphate or BeF_3^- bound as analogs of reaction intermediates (Rinaldo-Matthis et al., 2002), the phosphonate does not bind in a productive way for dephosphorylation. However, it is conceivable that if a phosphate instead of a phosphonate binds to the same site, it might be moved into a position productive for hydrolysis because of protein dynamics. Indeed, the only difference between the previously solved dNT-2 structures and the dNT-2–PMcP-U structure is the phosphonate part of the PMcP-U inhibitor that has moved 4 Å compared with the phosphate in the phosphate-containing structure (Fig. 1c). This suggests that this pocket has a very high affinity for the base and potentially also that the positioning of the base is the first event in the binding of substrates and nucleotide-based inhibitors. The observation that the (+) form and not its stereoisomer was bound in dNT-2 reflects the active site topology. Modeling of the (−) form of PMcP-U in the active site results in a steric clash between the base and the backbone carbonyl oxygen of residue 43 (not shown). The (+) form resembles the ribose ring more than the (−) form. The ribose ring of the product complex (Rinaldo-Matthis et al., 2002) and the cyclopentyl ring of the PMcP-U are stabilized by aromatic stacking interactions.

In contrast to PMcP-U, which inhibits both dNT-1 and dNT-2, DPB-T inhibits the dNT-2 enzyme only and with a mixed-type inhibition. The structure of the dNT-2-DPB-T complex reveals that bound DPB-T is more exposed to the solvent than the dNT-2 structures complexed with PMcP-U and thymidine (Figs. 1c and 2c) (Rinaldo-Matthis et al., 2002). Although the thymine base of DPB-T binds at almost the same place and with the same hydrogen bond interaction as the product (Rinaldo-Matthis et al., 2002) and the PMcP-U inhibitor (Fig. 2c), the rest of the molecule points toward the solvent, where the surface exposed Arg-163 and Lys-134 of the dNT-2 protein coordinate the phosphonate.

Although the thymine ring of DPB-T is still positioned in the base preferred binding pocket, the size, form, and freedom of bond rotations of the inhibitor seems to lack the conformational flexibility to bind with the phosphonate in the position occupied by the phosphate in the phosphate-containing structure. Surprisingly, a free phosphate is seen in the dNT-2-DPB-T structure complex, binding in the same place as the phosphate in the phosphate containing dNT-2 structure. The kinetics of mixed type inhibition of DPB-T relative to dUMP has a K_i of 70 μm (K_M for dUMP = 0.5 mM) and suggests two kinds of inhibition modes working simultaneously (Mazzon et al., 2003). One part is competitive, with the E+I complex blocking the formation of E+S. The other part of the inhibition is noncompetitive, which could be explained by the presence of the phosphate in the active site. The phosphate seen in the structure of the dNT-2-DPB-T complex probably comes from the crystallization buffer, because the crystals grow in presence of 50 mM KH_2PO_4. However, a free phosphate in the active site constitutes a late intermediate of the reaction, and the potential trapping of this intermediate by DPB-T-dNT-2 should be visible in the kinetics of inhibition. We have previously suggested a mechanism (Rinaldo-Matthis et al., 2002) by which the thymine product leaves the active site first and then the phosphate product. One possibility is that the DPB-T inhibitor binds to the intermediate [E+PO_4] and forms [EPO_4I] thereby blocking the dissociation of the phosphate (Scheme I). Thus, the catalytic rate would decrease, explaining the noncompetitive part of the inhibitory kinetics. Previous data on the inhibition of a different nucleotidase, CN-I, by different phosphonates support this view (Garvey et al., 1998).

The homologous protein dNT-1 is not inhibited by DPB-T. The analysis of the amino acid differences in the active sites of dNT-1 and dNT-2 clarify the structural basis for the difference in inhibition pattern of the two enzymes. A sequence alignment (Fig. 3) of the human deoxyribonucleotidases, together with a structural study of the differences, reveals why dNT-1 is not inhibited by DBP-T. The residues coordinating the phosphonate of DPB-T in dNT-2 are represented by ● and residues near the pentofuranosyl part of DPB-T are represented by △. All these residues are different in dNT-1. Of the four residues coordinating the base (Fig. 3, ▲) of the DPB-T inhibitor, three are conserved and Val-77 is replaced by Ala in dNT-1, a difference that does not contribute to the difference in inhibition pattern of DPB-T. Several other active site residues differ between dNT-1 and dNT-2 (Fig. 3); together, they may explain why dNT-1 is not inhibited by DBP-T.

The phosphono moieties of the two inhibitors as well as the phosphate in the phosphate containing structure, are found in different positions, but positively charged groups surround all three phosphates. In the dNT-2-DPB-T structure, Arg-163 coordinates the phosphonate group at the outside of the protein, suggesting a possible role of Arg-163 in the first recognition of the substrate phosphate moiety. In addition to Arg-163, Arg-177 and Lys-134 constitute a positively charged patch where the negatively charged phosphate of the substrate can bind to the protein. In the PMcP-U–dNT-2 structure, the phosphonate part of the molecule is making a hydrogen bond to Lys-165 and is positioned 8.6 Å deeper in the

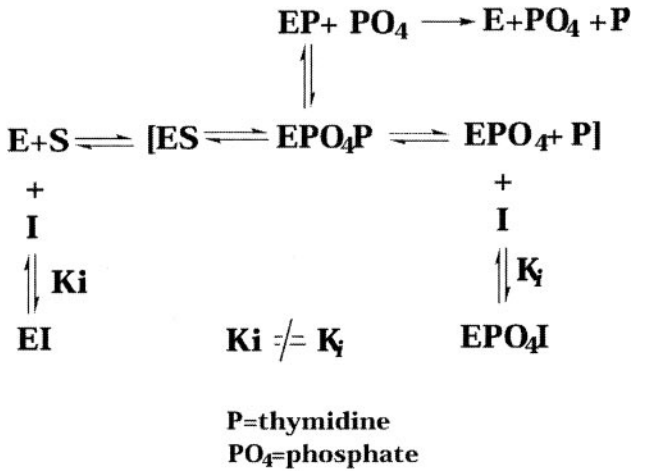

Scheme 1. Inhibition pattern of DPB-T with dNT-2. Both the competitive part of the inhibition and the noncompetitive part are shown. K_i is the dissociation constant for the free enzyme and the inhibitor whereas K_i represents the dissociation constant for the complex of enzyme-PO_4-inhibitor. The complex E-PO_4-I is what has been seen in the crystal structure of the DBP-T-dNT-2 structure complex. P is the thymidine product. Because the thymine base of the inhibitor binds in the active site where the substrates base is normally found, none of EIS or EIP is possible as intermediates, and in the structure we have caught the intermediate EPO_4I.

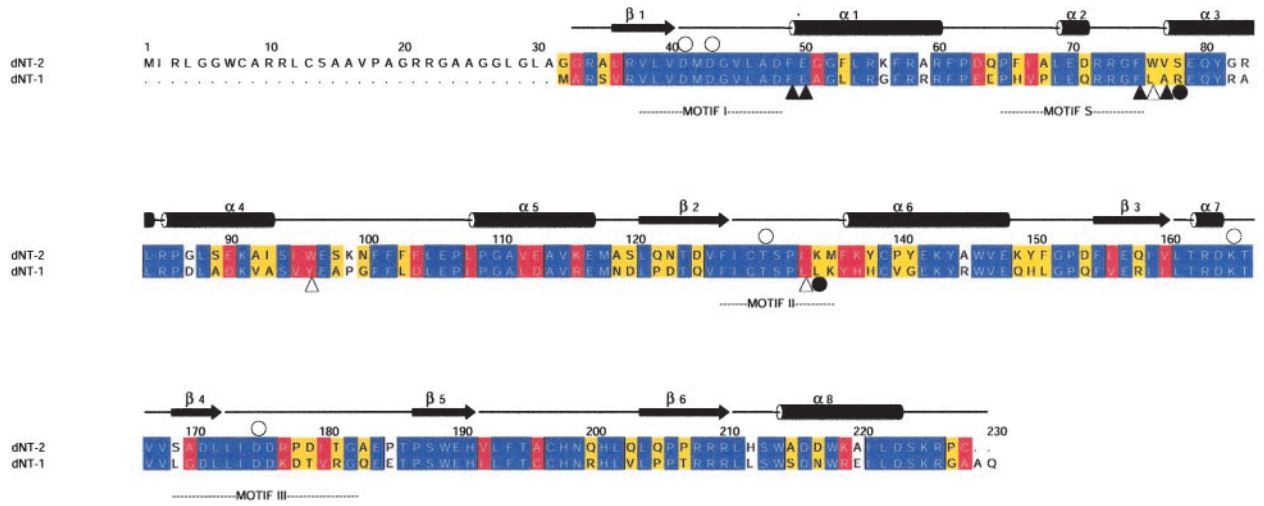

Fig. 3. Sequence alignment of the human dNT-2 (TrEMBL: Q9NPB1) and dNT-1 (TrEMBL: Q9NP82), sharing 50% sequence identity. The above numbering follows the amino acid sequence in dNT-2. Blue fields represent conserved residues, red fields represent residues with conserved mutations, yellow fields mark less conserved mutations than red fields, and white marks indicate no conservation at all. ○, amino acids involved in catalysis; ▲, residues interacting with the base; △, residues coordinating the pentofuranosyl part of DPB-T; ●, residues coordinating the phosphonate of DPB-T in dNT-2. The sequence alignment was done using ALSCRIPT (Barton, 1993) to clarify why dNT-1 is not inhibited by DBP-T inhibitor.

active site pocket compared with the position of the phosphonate of the DBP-T molecule. The positively charged Mg^{2+} as well as Lys-165 surround the third position binding of BeF_3^-, attached to the Asp-41 in the thymidine containing structure (Fig. 4). Residues enclosing the different positions of the phosphates in the three structures constitute a positively charged tunnel for the substrate to move through the active site to its productive position for hydrolysis, near Asp-41, as modeled by the structure complex of dNT-2-BeF_3-thymidine (Rinaldo-Matthis et al., 2002). Lys-165 might play an active role in positioning and stabilizing the phosphate before nucleophilic attack by Asp-41 because Lys-165 interacts with the phosphonate of PMcP-U and the BeF_3^- moiety. The observed binding modes of the inhibitors as well as the present "phosphate channel" suggest a number of potential modes for inhibitor development in the active site, making use of the residues interacting with the negatively charged oxygen atoms of the phosphate moieties (Fig. 4).

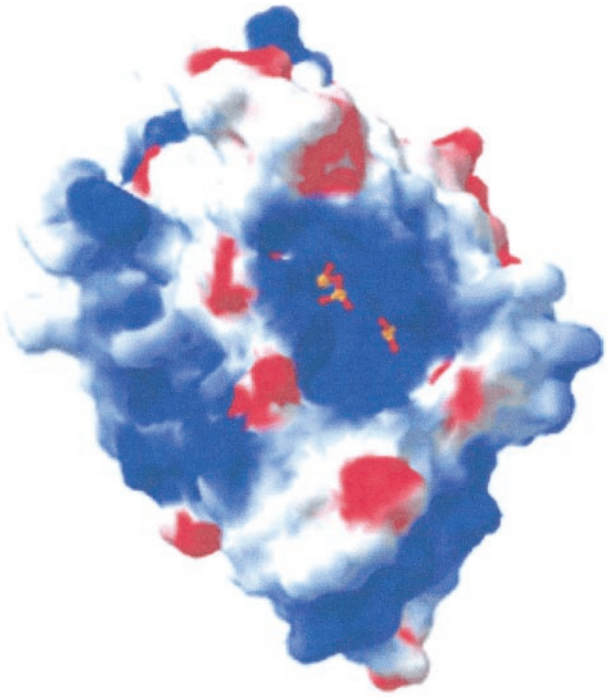

Fig. 4. Electrostatic potential surface of dNT-2 calculated using GRASP (Nicholls et al., 1991) together with two phosphonate binding sites from the inhibitors and one phosphate binding site from the phosphate containing structure. The three phospho binding sites constitute a positively charge tunnel from the surface into the active site, which could be functionally relevant for lowering the kinetic barrier for binding and releasing negatively charged moieties of substrates and products. Positively charged patches are shown in blue, and negatively charged patches are in red. The calculation is made by rolling a sphere of 1.4 Å on the surface of the protein.

Acknowledgments

We thank the staff at ESRF for technical assistance at ID14.2 and ID14.4. We are grateful to Karl-Magnus Larsson, Martin Högbom, and Pål Stenmark for help with data collection and Dave Stammers and Deborah Berthold for useful discussions on inhibitor kinetics. We also thank Fahmi Himo for help with geometry optimization of ligands.

References

Balzarini J, Aquaro S, Knispel T, Rampazzo C, Bianchi V, Perno CF, De Clercq E, and Meier C (2000). Cyclosaligenyl-2′,3′-didehydro-2′,3′-dideoxythymidine monophosphate: efficient intracellular delivery of d4TMP. *Mol Pharmacol* **58:**928–935.

Barton GJ (1993) ALSCRIPT: a tool to format multiple sequence alignments. *Protein Eng* **6:**37–40.

Brunger AT, Adams PD, Clore GM, DeLano WL, Gros P, Grosse-Kunstleve RW, Jiang JS, Kuszewski J, Nilges M, and Pannu NS (1998) Crystallography & NMR system: a new software suite for macromolecular structure determination. *Acta Crystallography D* **54:**905–921.

Carson DA, Carrera CJ, Wasson DB, and Iizasa T (1991) Deoxyadenosine-resistant human T lymphoblasts with elevated 5′-nucleotidase activity. *Biochim Biophys Acta* **1091:**22–28.

Dumontet C, Fabianowska-Majewska K, Mantincic D, Callet Bauchu E, Tigaud I, Gandhi V, Lepoivre M, Peters GJ, Rolland MO, Wyczechowska D, et al. (1999) Common resistance mechanisms to deoxynucleoside analogues in variants of the human erythroleukaemic line K562. *Br J Haematol* **106:**78–85.

Endová M, Masojídková M, Budìšínský M, and Rosenberg I (1998) 3′,5′-*O*-Phosphonoalkylidene derivatives of 1-(2-deoxy-β-D-*threo*-pentofuranosyl)thymine: synthesis and reactivity. *Tetrahedron* **54:**11187–11208.

Garvey EP, Lowen GT, and Almond MR (1998) Nucleotide and nucleoside analogues as inhibitors of cytosolic 5′-nucleotidase I from heart. *Biochemistry* **37:**9043–9051.

Gazziola C, Ferraro P, Moras M, Reichard P, and Bianchi V (2001) Cytosolic high K_m 5′-nucleotidase and 5′(3′)-deoxyribonucleotidase in substrate cycles involved in nucleotide metabolism. *J Biol Chem* **276:**6185–6190.

Hunsucker SA, Spychala J, and Mitchell BS (2001) Human cytosolic 5′-nucleotidase I: characterization and role in nucleoside analog resistance. *J Biol Chem* **276:**10498–10504.

Kleywegt GJ and Jones TA (1998) Databases in protein crystallography. *Acta Crystallogr Sec D* **54:**1119–1131.

Knofel T and Strater N (1999) X-ray structure of the *Escherichia coli* periplasmic 5′-nucleotidase containing a dimetal catalytic site. *Nat Struct Biol* **6:**448–453.

Kraulis P (1991) MOLSCRIPT: a program to produce both detailed and schematic plots of protein structures. *J Appl Cryst* **24:**946–950.

Laskowski RA, MacArthur MW, Moss DS, and Thornton JM (1993) PROCHECK: a program to check the stereochemical quality of protein structures. *J Appl Cryst* **26:**283–291.

Libosak R, Masojidkova M, and Rosenberg I (1996) Carbocyclic phosphonate-based nucleotide analogs related to PMEA. I. Racemic trans-configured derivatives. *Collect Czech Chem Commun* **61:**313–317.

Lim SE and Copeland WC (2001) Differential incorporation and removal of antiviral deoxynucleotides by human DNA polymerase γ. *J Biol Chem* **276:**23616–23.

Mazzon C, Rampazzo C, Scaini MC, Gallinaro L, Karlsson A, Meier C, Balzarini J, Reichard P, and Bianchi V (2003) Cytosolic and mitochondrial deoxyribonucleotidases: activity with substrate analogs, inhibitors and implications for therapy. *Biochem Pharmacol* **66:**471–479.

Merritt EA (1999) Expanding the model: anisotropic displacement parameters in protein structure refinement. *Acta Crystallogr Sec D* **55:**1109–1117.

Murshudov GN, Vagen AA, and Dodson EJ (1997) Refinement of macromolecular structures by the maximum-likelihood method. *Acta Crystallogr Sec D* **53:**240–255.

Nicholls A, Sharp KA, and Honig B (1991) Protein folding and association: insights from the interfacial and thermodynamic properties of hydrocarbons. *Proteins* **11:**281–296.

Nishino I, Spinazzola A, and Hirano M (1999) Thymidine phosphorylase gene mutations in MNGIE, a human mitochondrial disorder. *Science (Wash DC)* **283:**689–692.

Otwinowski Z and Minor W (1997) Processing of x-ray diffraction data collected in oscillation mode, in *Macromolecular Crystallography. Part A* (Carter CW Jr, Sweet RM eds) Methods in Enzymology, vol 276. Academic Press, San Diego, CA.

Rampazzo C, Gallinaro L, Milanesi E, Frigimelica E, Reichard P, and Bianchi V (2000) A deoxyribonucleotidase in mitochondria: involvement in regulation of dNTP pools and possible link to genetic disease. *Proc Natl Acad Sci USA* **97:**8239–8244.

Rampazzo C, Mazzon C, Reichard P, and Bianchi V (2002) 5′-Nucleotidases: specific assays for five different enzymes in cell extracts. *Biochem Biophys Res Commun* **293:**258–263.

Rinaldo-Matthis A, Rampazzo C, Reichard P, Bianchi V, and Nordlund P (2002) Crystal structure of a human mitochondrial deoxyribonucleotidase. *Nat Struct Biol* **9:**779–787.

Sala-Newby GB and Newby AC (2001) Cloning of a mouse cytosolic 5′ nucleotidase-I identifies a new gene related to human autoimmune infertility-related protein. *Biochim Biophys Acta* **1521:**12–18.

Schirmer M, Stegmann AP, Geisen F, and Konwalinka G (1998) Lack of cross-resistance with gemcitabine and cytarabine in cladribine-resistant HL60 cells with elevated 5′-nucleotidase activity. *Exp Hematol* **26:**1223–1228.

Wallace AC, Laskowski RA, and Thornton JM (1995) LIGPLOT: a program to generate schematic diagrams of protein-ligand interactions. *Protein Eng* **8:**127–134.

Address correspondence to: P. Nordlund, Dept. of Biochemistry and Biophysics, Stockholm University, S-106 91 Stockholm, Sweden. E-mail: par@dbb.su.se